The Stability of a Developing Thermal Front in a Porous Medium. II Nonlinear Evolution

Asma Selim and D. Andrew S. Rees

Department of Mechanical Engineering, University of Bath, Bath BA2 7AY, UK

ABSTRACT

We consider the instability of the unsteady thermal boundary that is caused by suddenly raising the temperature of the lower boundary of an otherwise cold saturated porous medium. In particular, we focus attention on strongly nonlinear two-dimensional convection. A comprehensive set of results is presented which shows the effects of varying the amplitude of the disturbance, its wave number, and the time at which the disturbance is introduced into the developing thermal boundary layer. We indicate, in detail, how the evolution of the instabilities with time is affected by nonlinearity and how the characteristics of that evolution are changed from those that arise in linearized theory. We also determine when linearized theory is inadequate to describe the global features of the evolution, such as the restabilisation of convection.

17

NOMENCLATURE

A	amplitude of disturbance
g	gravity
k	wavenumber of disturbance
K	permeability
L	natural length scale
n	summation index
n_1, n_2	summation indices
N	number of Fourier modes
p, P	pressure
q	surface rate of heat transfer
t	time
T	dimensional temperature
T_w	lower surface temperature
T_∞	ambient temperature
u	horizontal velocity
v	vertical velocity
x	horizontal coordinate
y	vertical coordinate

Greek characters

α	thermal diffusivity
β	coefficient of thermal expansion
ΔT	temperature difference
η	similarity variable
θ	nondimensional temperature
μ	dynamic viscosity
ρ	density
τ	$= \sqrt{t}$
ψ	streamfunction

Superscripts and subscripts

$-$	dimensional
0	initial disturbance
nl	nonlinear stability criterion

INTRODUCTION

In Selim and Rees (2007), herein referred to as Part I, we studied the linear instability of the developing conduction profile, which is induced by the sudden rise in temperature of the horizontal lower boundary of an otherwise unbounded porous medium that is saturated and uniformly cold. The developing thermal field is given by the complementary error function, and there is no flow. As the lower boundary is relatively hot, light fluid lies below relatively heavy fluid, and there is the potential for thermoconvective instability. It was pointed out in Part I that a Darcy-Rayleigh number based on the thickness of this developing thermal front always rises, and therefore, it is to be expected that the developing thermal front will eventually become unstable.

In Part I, attention was focused on how different wave numbers, initiation times, and initial profiles of the disturbance affect the evolution of the disturbance. Particular attention was paid to determining stability criteria based on various measures of the strength of the disturbance, and on how these stability criteria compare to approximate quasi-steady theory.

A few papers exist that deal with the instability of a time-dependent boundary layer in porous media. Kaviany (1984) considered internal heat generation in a finite thickness layer as an unsteady problem. On employing the Forchheimer-Brinkman-extended Darcy model for the momentum equation, he allowed the upper boundary temperature to decrease linearly with time, and obtained stability criteria using approximate methods. A different type of unsteady problem with

heat generation was considered by Kim et al. (2002), who used a suddenly imposed internal heat generation as the unsteady feature, and the basic thermal state then varied from a uniformly cold temperature. Later, Kim et al. (2003) considered a very similar problem to the one considered here, except that, as shown in Part I, their momentum boundary conditions allow for zero tangential velocity rather than a zero normal velocity at the lower boundary. In a recent paper, Kim and Kim (2005) have undertaken a study of a ramp heating case, where the temperature of the lower surface increases linearly with time in a layer of finite depth. But in the first three of the papers quoted in this paragraph approximate linearized theories were employed to generate stability criteria.

In this paper, we extend the analysis of Part I into the nonlinear regime in order to determine how finite amplitude disturbances evolve. We use a method that is a mixed finite difference and Fourier series expansion, and the resulting system of equations is solved using a slightly modified form of the Keller-box method (Keller and Cebeci, 1971). We have available three main parameters to vary, namely, the wave number of the primary mode, its amplitude, and its initiation time. We present a fairly comprehensive account of how the subsequent evolution of the disturbance depends on these parameters. Our general aim is to find the similarities and differences between the linear and nonlinear characteristics and to determine when nonlinear effects are significant.

GOVERNING EQUATIONS AND BASIC SOLUTION

Consider the free convective flow above a horizontal impermeable surface embedded in a fluid-saturated porous medium, where the medium is considered to be isotropic and homogeneous and where the fluid and the porous matrix are in local thermal equilibrium. Non-Darcy effects, as modeled by the Brinkman and Forchheimer terms, are neglected for now. The porous medium is considered to be quiescent initially and uniformly cold. At the time $t = 0$, the temperature of

the bounding horizontal surface is raised suddenly to a new constant level at which it remains for all $t > 0$. The governing equations are taken to be Darcy's law modified by the presence of buoyancy and subject to the Boussinesq approximation, the equation of continuity and the thermal energy equation:

$$\frac{\partial \overline{u}}{\partial \overline{x}} + \frac{\partial \overline{v}}{\partial \overline{y}} = 0 \tag{1a}$$

$$\overline{u} = -\frac{K}{\mu}\frac{\partial \overline{P}}{\partial \overline{x}} \tag{1b}$$

$$\overline{v} = -\frac{K}{\mu}\frac{\partial \overline{P}}{\partial \overline{y}} + \frac{\rho g \beta K}{\mu}(T - T_\infty) \tag{1c}$$

$$\frac{\partial T}{\partial \overline{t}} + \overline{u}\frac{\partial T}{\partial \overline{x}} + \overline{v}\frac{\partial T}{\partial \overline{y}} = \alpha\left(\frac{\partial^2 T}{\partial \overline{x}^2} + \frac{\partial^2 T}{\partial \overline{y}^2}\right) \tag{1d}$$

In these equations, $\overline{x}$ is the coordinate in the horizontal direction while $\overline{y}$ is vertically upward. The corresponding velocities are $\overline{u}$ and $\overline{v}$, respectively. All the other terms have their usual meaning for porous medium convection: K is the permeability, μ is the dynamic viscosity, and ρ is the density of the fluid at the ambient temperature, $T = T_\infty$. The heated horizontal surface is held at the temperature T_w, where $T_w > T_\infty$. Finally, the quantities g, β, and α are gravity, the coefficient of cubical expansion, and the thermal diffusivity of the saturated medium, respectively.

Equations (1a)–(1d) may now be nondimensionalised using the following transformations:

$$\bar{t} = \frac{L^2}{\alpha}t, \quad (\overline{x}, \overline{y}) = L(x, y)$$

$$(\overline{u}, \overline{v}) = \frac{\alpha}{L}(u, v)$$

$$\overline{P} = \frac{\alpha\mu}{K}p, \quad T = T_\infty + \Delta T\,\theta \tag{3}$$

to yield

$$\frac{\partial u}{\partial x} + \frac{\partial v}{\partial y} = 0 \tag{2a}$$

$$u = -\frac{\partial p}{\partial x} \tag{2b}$$

$$v = -\frac{\partial p}{\partial y} + \theta \tag{2c}$$

$$\frac{\partial \theta}{\partial t} + u\frac{\partial \theta}{\partial x} + v\frac{\partial \theta}{\partial y} = \frac{\partial^2 \theta}{\partial x^2} + \frac{\partial^2 \theta}{\partial y^2} \tag{2d}$$

The appropriate boundary conditions are

$$y = 0 : v = 0, \quad \theta = 1 \qquad \text{and}$$
$$y \to \infty : v, \qquad \theta \to 0 \tag{2e}$$

while $\theta = 0$ everywhere for $t < 0$. We note that there is no Darcy-Rayleigh number present in Eqs. (2). As discussed in Part 1, the reason is simply that there is no external length scale present in a semi-infinite medium, and therefore, setting the Darcy-Rayleigh number, $\mathrm{Ra} = \rho g \beta K L (T_w - T_\infty)/\mu\alpha$, to be equal to unity is equivalent to defining a lengthscale, L, in terms of the properties of the porous medium and the saturating fluid.

After eliminating the pressure p between Eqs. (3b) and (3c), and on introducing the streamfunction ψ, defined according to

$$u = -\frac{\partial \psi}{\partial y} \qquad \text{and} \qquad v = \frac{\partial \psi}{\partial x} \tag{3}$$

then the continuity equation is satisfied, and Eqs. (3b)–(3d) reduce to the pair,

$$\frac{\partial^2 \psi}{\partial x^2} + \frac{\partial^2 \psi}{\partial y^2} = \frac{\partial \theta}{\partial x} \tag{4a}$$

$$\frac{\partial \theta}{\partial t} + \frac{\partial \psi}{\partial x}\frac{\partial \theta}{\partial y} - \frac{\partial \psi}{\partial y}\frac{\partial \theta}{\partial x} = \frac{\partial^2 \theta}{\partial x^2} + \frac{\partial^2 \theta}{\partial y^2} \tag{4b}$$

where ψ is the streamfunction, which is defined according to $u = -\frac{\partial \psi}{\partial y}$ and $v = \frac{\partial \psi}{\partial x}$, and where the appropriate boundary conditions are

$$y = 0 : \psi = 0, \quad \theta = 1 \qquad \text{and}$$
$$y \to \infty : \psi, \qquad \theta \to 0 \tag{4c}$$

The initial state is

$$\psi = \theta = 0 \quad \text{for} \quad t \leq 0 \tag{4d}$$

The basic state whose nonlinear stability is being considered is one of pure conduction with no flow, and this is given by,

$$\psi = 0, \quad \theta = \mathrm{erfc}(\eta) = \frac{2}{\sqrt{\pi}} \int_\eta^\infty e^{-\xi^2}\, d\xi \tag{5}$$

where η is the similarity variable defined as

$$\eta = \frac{y}{2\sqrt{t}} \tag{6}$$

Equations (4a) and (4b) may now be transformed into the coordinate system (η, τ), where $\tau = \sqrt{t}$; we obtain

$$4\tau^2 \frac{\partial^2 \psi}{\partial x^2} + \frac{\partial^2 \psi}{\partial \eta^2} = 4\tau^2 \frac{\partial \theta}{\partial x} \tag{7a}$$

$$2\tau \frac{\partial \theta}{\partial \tau} + 2\tau \left(\frac{\partial \psi}{\partial x}\frac{\partial \theta}{\partial \eta} - \frac{\partial \psi}{\partial \eta}\frac{\partial \theta}{\partial x} \right)$$
$$= 4\tau^2 \frac{\partial^2 \theta}{\partial x^2} + \frac{\partial^2 \theta}{\partial \eta^2} + 2\eta \frac{\partial \theta}{\partial \eta} \tag{7b}$$

As in Part I, we note that the coefficient of $\partial\theta/\partial x$ on the right-hand side of (7a) may be regarded as a "local" Darcy-Rayleigh number, and therefore, the system becomes increasingly thermoconvectively unstable with time.

NUMERICAL METHOD

The full linearized disturbance equations were solved numerically in Part I using a parabolic solver to determine stability criteria. These results were compared with an approximate theory obtained by neglecting the time derivative and nonlinear terms in (7b) and regarding τ as an eigenvalue, which is itself a function of k, the wave number. We are now interested in investigating, numerically how the evolution of the disturbance changes when nonlinearity is significant. To this end, a truncated spanwise Fourier expansion of the form

$$\psi(x, \eta, \tau) = \sum_{n=1}^{N} \psi_n(\eta, \tau) \sin nkx \tag{8a}$$

$$\theta(x, \eta, \tau) = \mathrm{erfc}(\eta) + \frac{1}{2}\theta_0(\eta, \tau)$$
$$+ \sum_{n=1}^{N} \theta_n(\eta, \tau) \cos nkx \tag{8b}$$

is substituted into Eqs. (7a) and (7b). We refer to ψ_1 and θ_1 as the primary mode, as these terms correspond to the disturbances studied in Part I. The term $\frac{1}{2}\theta_0$ yields the mean change to the basic state due to the presence of convective cells. In general, the pair (ψ_n, θ_n) is referred to as mode n.

The detailed equations corresponding to each pair, (ψ_n, θ_n), are quite lengthy, especially if N, the number of modes chosen, is large, and therefore, they are omitted here. Indeed, it was not even necessary to write down the detailed expansions for the nonlinear terms, for our implementation of the Keller-box code was able to account for these nonlinear interactions automatically. For example, the expression, $(n_1 k \psi_{n_1} \cos n_1 kx)(\theta_{n_2,\eta} \cos n_2 kx)$, arises as one of the products resulting from the first nonlinear term in (7b), where n_1 and n_2 are arbitrary values of the summation indices in (7a) and (7b), respectively. This term may be written in the form

$$
\begin{aligned}
n_1 k\, \psi_{n_1} & \frac{\partial \theta_{n_2}}{\partial \eta} \cos(n_1 kx) \cos(n_2 kx) \\
&= \frac{1}{2} n_1 k \Big\{ \cos\big[(n_1 + n_2)kx\big] \\
&+ \cos\big[(n_1 - n_2)kx\big] \Big\} \psi_{n_1} \frac{\partial \theta_{n_2}}{\partial \eta} \qquad (9)
\end{aligned}
$$

If a double loop is written where both n_1 and n_2 run from 1 to N; then the coefficient of $\cos(n_1 + n_2)kx$ in (9) is added to the accumulating sum of terms that need to be included in the equation for $\theta_{n_1+n_2}$, should $n_1 + n_2 \leq N$; otherwise, they are ignored. Likewise, the full coefficient of $\cos(n_1 - n_2)kx$ is added to the accumulating sum of terms for the equation for $\theta_{|n_1-n_2|}$.

In the numerical simulations, the truncation level was chosen to be $N = 5$, which was sufficent for the present purpose, for the magnitude of θ_5 was always very small compared with unity. After the substitution of Eqs. (8) into Eqs. (7), the final system consists of $2N + 1$ second-order partial differential equations in τ and η, which forms a parabolic system. This system is solved by a slightly modified Keller-box method. The standard Keller-box methodology first reduces the whole system to one involving equations, which are of first order in η. Then a central difference in time based half way between the time steps is used. Finally, the resulting nonlinear difference equations are solved iteratively using a multidimensional Newton-Raphson scheme. For the present problem, with $N = 5$, this would mean that a nonlinear system of 22 difference equations would need to be solved. We chose to modify the Keller-box methodology in two ways: (i) the partial differential equations were kept in second-order form in η and (ii) backward differences in time were adopted. The first modification means that there are now only 11 difference equations, which results in a much faster computation. It also means that the iteration matrix retains block tridiagonal form, and therefore, the modification to standard Keller-box code is very straightforward. The second modification means that numerical stability is increased with no possibility of pointwise oscillations, while still requiring only straightforward changes to a standard Keller-box code. In addition to these modifications, the numerical differentiation methodology used by Lewis et al. (1997) was also implemented to evaluate the iteration matrix, which would otherwise be extremely lengthy to encode explicitly.

A rectangular domain in η and τ was used in the whole simulation where η ranges from 0 to 10 with the uniform step of 0.05, and a steplength of 0.1 was used in the τ direction. As in Part I, a thermal disturbance is introduced at $\tau = \tau_0$, the initiation time, and the Keller-box method is then used to march the disturbance forward in time. In the linearized theory of Part I, the evolving disturbance is a function solely of k and τ_0, but here the evolution also depends on the magnitude of the disturbance. In this paper, we introduce disturbances in the form $\theta_1 = A\eta e^{-3\eta}$, where A is the amplitude of the disturbance. This profile was taken as the datum profile in Part I, and it was shown there that the time at which disturbances begin to grow is generally independent of the profile shape and the initiation time if the disturbance is introduced before $\tau \simeq 5$.

We reproduce the neutral stability curve of Part I in Fig. 1; this was the result of solving the quasi-steady ordinary differential eigenvalue problem for the critical time and is shown here as the context into which to set the present nonlinear computations. Disturbances decay that correspond to locations below the curve, to the right of the right-hand branch and to
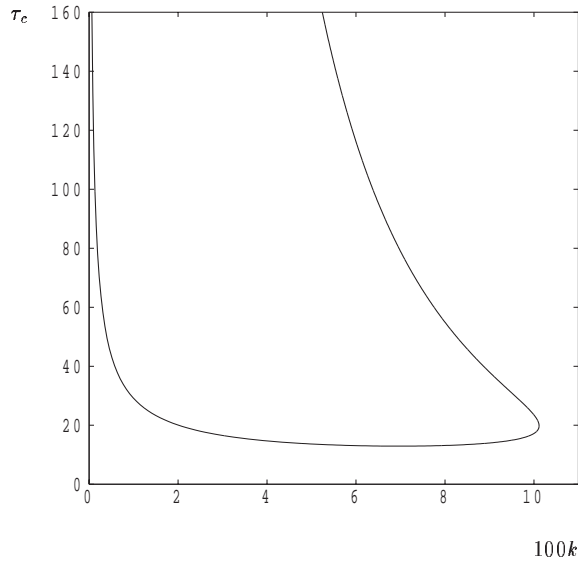
Figure 1. Neutral stability curve displaying the critical time τ_c against the wave number, k

the left of the left-hand branch; otherwise, they grow (i.e., are unstable). Part I also showed that a thermal energy-based criterion for monitoring the growth of the disturbance results in a larger region of instability than is indicated in Fig. 1.

NUMERICAL RESULTS

In this section, we discuss, in detail, how the nonlinear evolution of disturbances is affected by changes in the wave number k, the amplitude A, of the disturbance, and the initiation time τ_0. However, it is necessary to show first some of the general features of how a disturbance evolves when in the nonlinear regime, emphasizing, in particular, those ways in which the evolution is different from that of linear theory, which is based on infinitesimal disturbances. The most frequently used measure of the strength of the disturbance is the surface rate of heat transfer, and therefore, we define

$$q_n = \frac{\partial \theta_n}{\partial \eta}\Big|_{\eta=0} \tag{10}$$

to be the rate of heat transfer for mode n. The variation with τ of q_1 determines how the primary

mode is evolving, whereas $\frac{1}{2}q_0$ shows the evolution of the mean rate of heat transfer per spanwise wavelength. The value of $\frac{1}{2}q_0$ should be compared with $-2/\sqrt{\pi} = -1.1284$, which is the rate of heat transfer of the basic temperature profile given in Eq. (5).

A typical case

Figure 2 represents the variation of q_n with τ for $n = 0, 1, \ldots, 5$ for a disturbance that is introduced at $\tau_0 = 8$, with the wave number $k = 0.05$ and the amplitude $A = 10^{-1}$. First, it is essential to point out that the choice of the truncation level, $N = 5$, in Eqs. (8), is justified by the curves shown in this figure, where the $n = 4$ curve can only just be distinguished from the τ-axis.

At first, the value of q_1 decays in accordance with linear theory since τ_0 lies well below the neutral curve for this wave number. When $\tau \simeq 20$, the value of q_1 begins to grow, which is again in agreement with linear theory. However, the results of Part I indicate that the amplitude of such a growing mode will increase through many orders of magnitude as τ in-
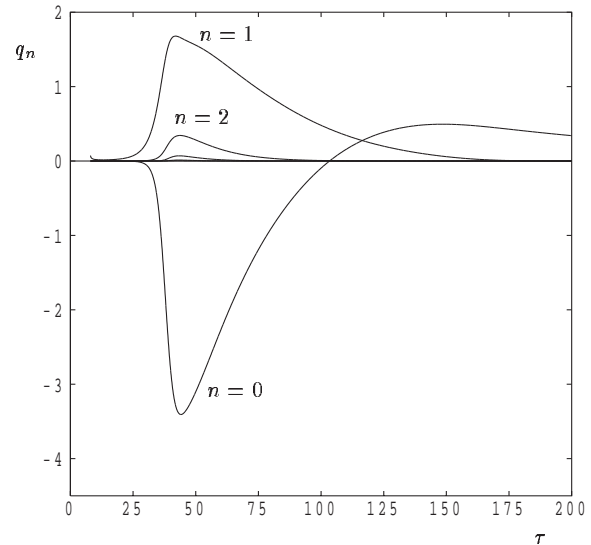
Figure 2. Variation with τ of the surface rates of heat transfer, q_n, corresponding to the Fourier modes, $n = 0, 1, 2, \ldots$ We have taken $\tau_0 = 8$, $k = 0.05$ and $A = 10^{-1}$

creases. In the present case, nonlinear self-interactions of the growing disturbance induces flow corresponding to the $n = 0$ and $n = 2$ modes, and then further interactions cascade through the higher modes. This is seen clearly in Fig. 2, where there are rapid increases in q_1 and q_2 up to $\tau \simeq 40$. At the same time, the mean rate of heat transfer q_0 attains quite a large negative value. At its maximum magnitude, the value of $\frac{1}{2}q_0$ is such that the mean heat transfer has increased to a value that is more than twice that of the basic state. After this maximum has been reached, all the modes begin to decay slowly, suggesting that the flow is restabilizing. This conclusion, while clearly consistent with the curves shown in Fig. 2, is at variance with the linear stability theory, as displayed in Fig. 1, which indicates that a $k = 0.05$ disturbance should continue to grow until well after $\tau = 160$. Therefore, we must have a situation where the evolving cells display a nonlinear saturation. An alternative way of looking at this is based on the fact that the mean temperature profile has changed from $\mathrm{erfc}\,(\eta)$ to $\mathrm{erfc}\,(\eta) + \frac{1}{2}\theta_0$. Therefore, it is to be expected that linear theory, which is based on disturbances to the basic profile, cannot apply in such a highly nonlinear situation where the mean state is now very different.

An different view of the development of the disturbance is shown in Fig. 3, which displays isotherms and streamlines of the evolving disturbance at various values of τ for the wave number $k = 0.05$. Each subframe of Fig. 3 shows one period in the x direction. The middle cell of each subframe of Fig. 3a corresponds to a negative temperature disturbance, and there is fluid flow directed toward the heated surface. Thus, the streamlines placed midway between the vertical borders of each subframe of Fig. 3b correspond to inflow. The outer cells, on the other hand, are positive perturbations and the vertical borders of the streamline plots represent outflow streamlines.

For $\tau \le 30$, the disturbance gradually becomes narrower in terms of η as it develops, just as disturbances do within the linear regime. This effect is seen more clearly in the streamlines, where the exponen-

tional decay of Ψ may be shown to be proportional to $\exp(-2k\tau\eta)$, and therefore, the e–folding distance decreases with τ. However, at later times, nonlinear effects become significant. The first sign of nonlinearity is that neighbouring thermal cells no longer resemble one another, as seen in Fig. 3a when $\tau = 40$. As the edges of the subframes are the streamlines corresponding to outflow, where the fluid is warmer than the basic state, we see the centers of the thermal disturbances becoming displaced further away from the heated surface. Conversely, the central cell is being pushed toward the heated surface due to the strength of the inflow midway between the two outflow streamlines. The central cell now begins to adopt a triangular shape because its neighbouring cells have risen up from the heated surface, and the increased density of the isotherms together with the spreading of the cell near the surface indicates why there is a large increase in the magnitude of the mean rate of heat transfer at this time. At later times, such as $\tau = 100$, the magnitude of the primary cell has decreased to such an extent that the isotherms are almost dominated by the mean disturbance θ_0, which is still large but is now decaying, as seen in Fig. 2. The streamlines also occupy a decreasingly sized region in terms of η as τ continues to grow.

Effect of varying the wave number

In this section, we concentrate on the effect of varying the wave number on the evolution of disturbances within the nonlinear regime. Figure 4 shows how q_1 varies with τ for a selection of wave numbers between 0.04 and 0.09, inclusive, for both $A = 10^{-1}$ and $A = 10^{-4}$. The disturbance was initiated at $\tau_0 = 8$. All the disturbances decay immediately on introduction, but then begin to grow again at a value of τ, which is broadly in line with linear theory. Of the curves shown in Fig. 4a, for $A = 10^{-1}$, only those corresponding to $k = 0.08$ and $k = 0.09$ have the property that the disturbance restabilizes at a value of τ that is roughly the same as given by the upper branch of Fig. 1. The reason is simply that the
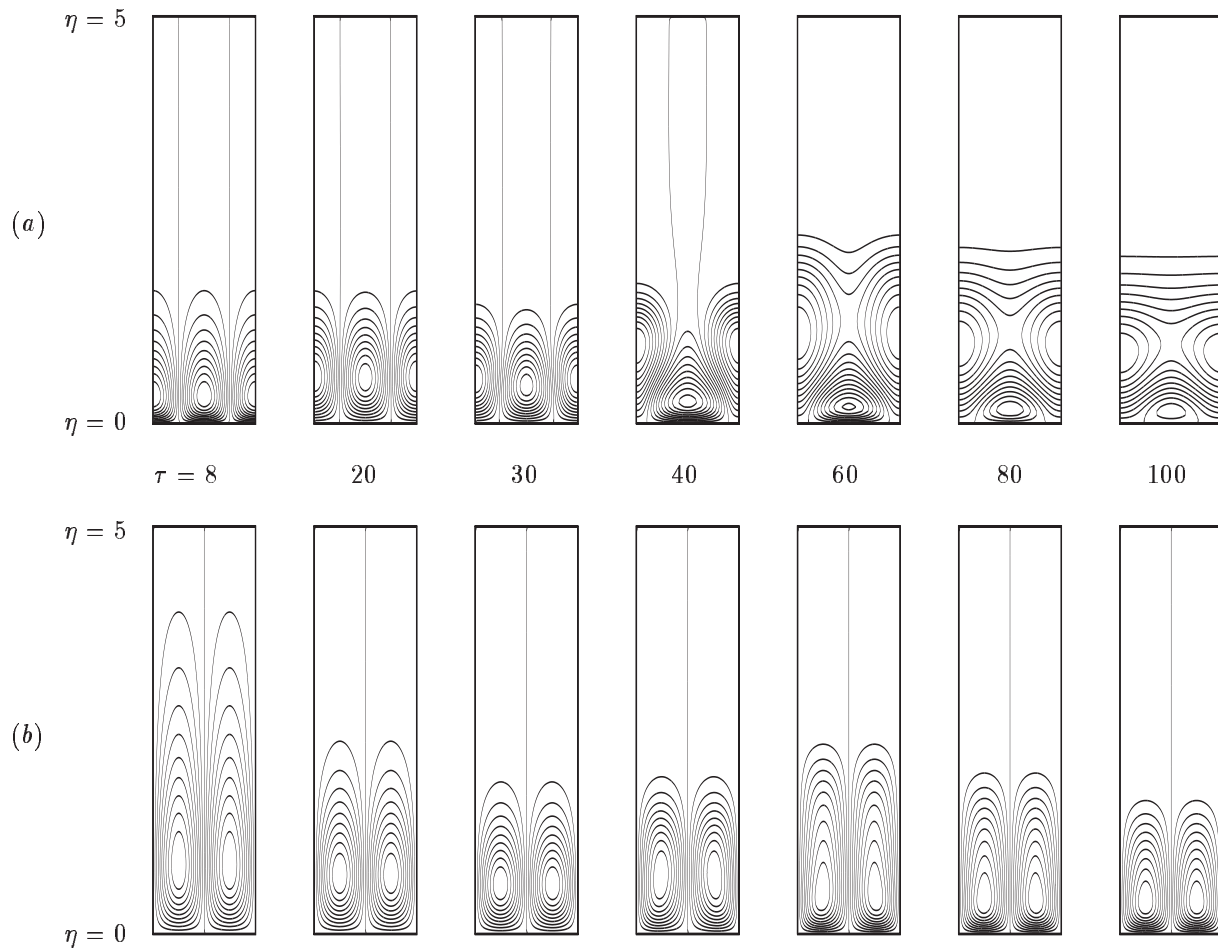
Figure 3. Cross section of the convection cells corresponding to **a)** the perturbation temperature profiles and **b)** the streamlines, for various values of τ using $\tau_0 = 8$, $k = 0.05$, and $A = 10^{-1}$

interval of time over which the disturbances grow is sufficiently short that nonlinearities do not become significant, and therefore, linearized theory applies fairly accurately. For the other wave numbers, restabilization is predicted to take place at increasing values of τ, as shown by Fig. 1, but, for the choice of τ_0 and A used here, restabilization is confined to the range $40 < \tau < 45$ almost independently of the value of k. Again, premature restabilization is due to nonlinear saturation and a highly modified mean flow and temperature field.

Figure 4b shows the situation that applies when the disturbance amplitude is reduced to 10^{-4}. The

detailed numerical data again show that onset occurs at a time broadly in line with Fig. 1, but now a substantially longer period of time is required before the disturbance attains an O(1) magnitude. Apart from the $k \geq 0.07$ cases, which are essentially linear, a rapid growth to a maximum response is followed by an almost equally rapid decay, and the time of maximum response is again roughly constant for the smaller wave numbers.
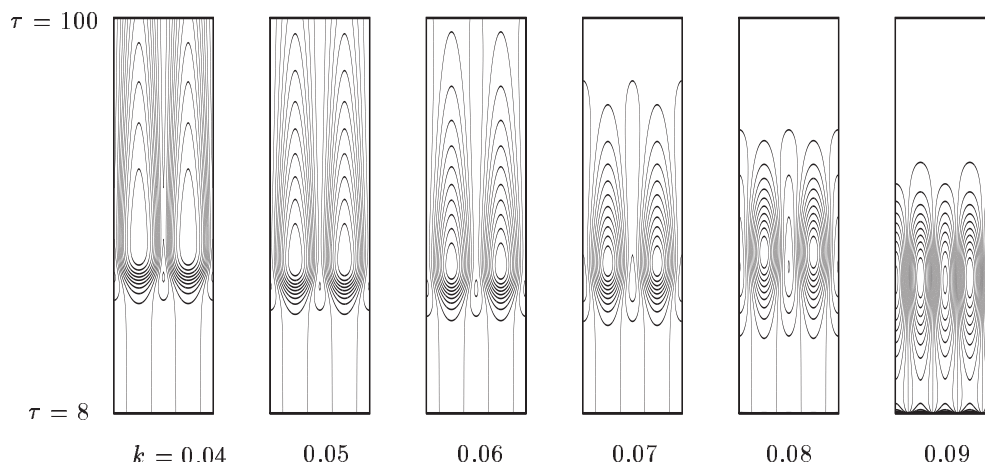
The isolines of the rate of surface heat transfer corresponding to the different wave numbers considered in Fig. 4a are shown in Fig. 5. These isolines are equally spaced between $\pm$max $|q_1|$, and two whole
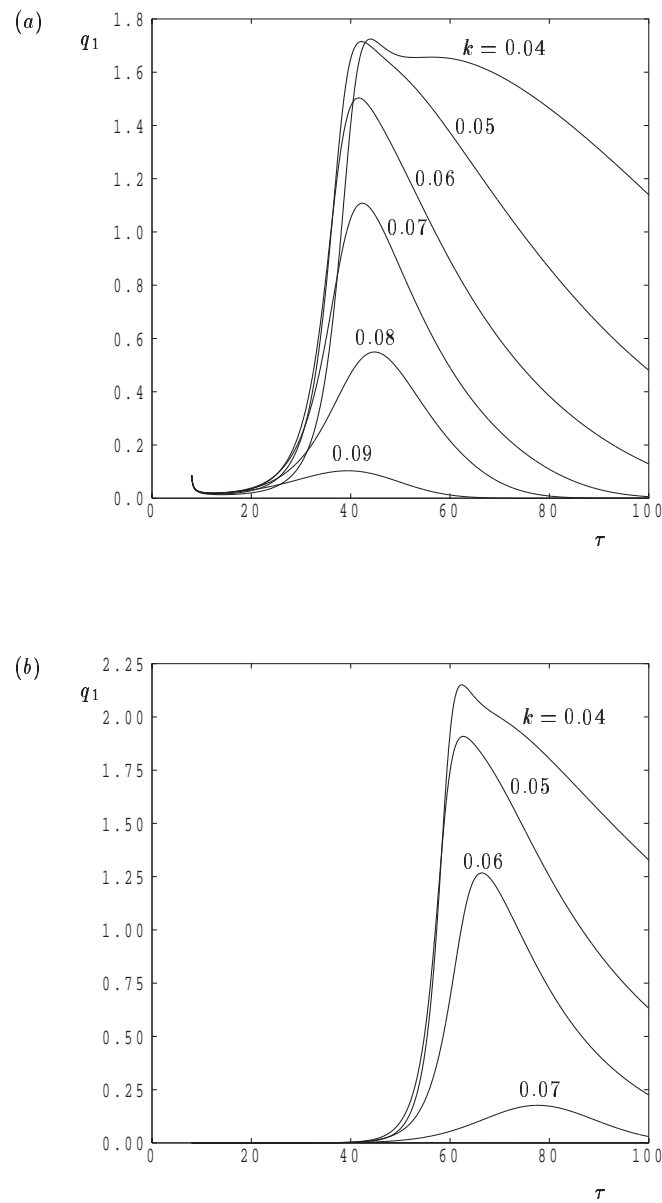
Figure 4. Variation in the surface rate of heat transfer, q_1, due to the primary cell for various wave numbers and for $\tau_0 = 8$: **a)** $A = 10^{-1}$, **b)** $A = 10^{-4}$

periods in the spanwise direction are shown for in-creased clarity. For $k = 0.09$, the near linearity of the response to the disturbance may be guaged by seeing how similar the isolines of surface heat transfer of neighbouring thermal cells are to each other. Neigh-bouring cells are more dissimilar for $k = 0.08$, but this dissimilarity is still fairly weak, given that the time of restabilization is still close to that given by linear theory. For the remaining three cases, nonlinear effects are very strong. The presence of the central cells is hidden when $\tau > 40$, for these cells are the ones that rise away from the surface due to outflow.

Figure 5. Isolines of the surface rate of heat transfer in (τ, x)-space for various values of the vortex wave number k, using $\tau_0 = 8$ and $A = 10^{-1}$. The horizontal coordinate varies between $x = 0$ and $x = 4\pi/k$, i.e., two horizontal periods are displayed

The strong sets of contours that remain correspond to those cells that are pressed against the surface by inflow and have triangular cross section.

Varying the disturbance amplitude

Although we may compare Figs. 4a and 4b, a more comprehensive approach to finding the effects of varying the disturbance amplitude is presented here. It is to be expected that different disturbance amplitudes will result in quite different consequences once the evolving disturbance is strong enough to generate harmonics. The degree to which this happens is the subject of this section and demonstrated in Figs. 6 and 7.

Figure 6 gives a comprehensive account of the detailed response to variations in the amplitude of the disturbance A for a selection of wave numbers. In particular, the evolution with τ of both q_1 and q_0 are shown, and the disturbance amplitudes chosen vary in inverse integer powers of 10 from $A = 10^{-1}$ down to $A = 10^{-20}$. We note, in passing, that the convergence criterion for each value of τ in our numerical simulation is a relative criterion, rather than an absolute criterion, i.e., convergence is deemed to

have taken place when the maximum change between successive iterates divided by the maximum value of the iterate is $< 10^{-8}$. Therefore, we have roughly eight significant figures, even when the disturbances are extremely small.

A brief glance at the behaviour of both q_1 and q_0 is sufficient to note that nonlinear saturation depends very strongly on the disturbance amplitude, and, not surprisingly, the time at which saturation occurs becomes later as the value of A decreases. What is surprising, however, is that the largest disturbance amplitudes do not yield the largest response. Taking the case $k = 0.04$, for example, $A = 10^{-12}$ yields the largest response in q_1, whereas, for $k = 0.05$, the largest response is obtained when $A = 10^{-4}$. For larger wave numbers, the time available for the disturbance to grow is limited by the upper branch of the neutral curve, and it is not possible for the disturbance to become particularly large before it begins to decay again. This effect may be seen clearly when comparing the times of restabilization of the $A = 10^{-8}$ and $A = 10^{-9}$ cases for $k = 0.06$, and the $A = 10^{-4}$ and 10^{-5} cases for $k = 0.07$. For these larger wave numbers, the largest response is obtained from the largest disturbance amplitudes. When $k = 0.08$ and
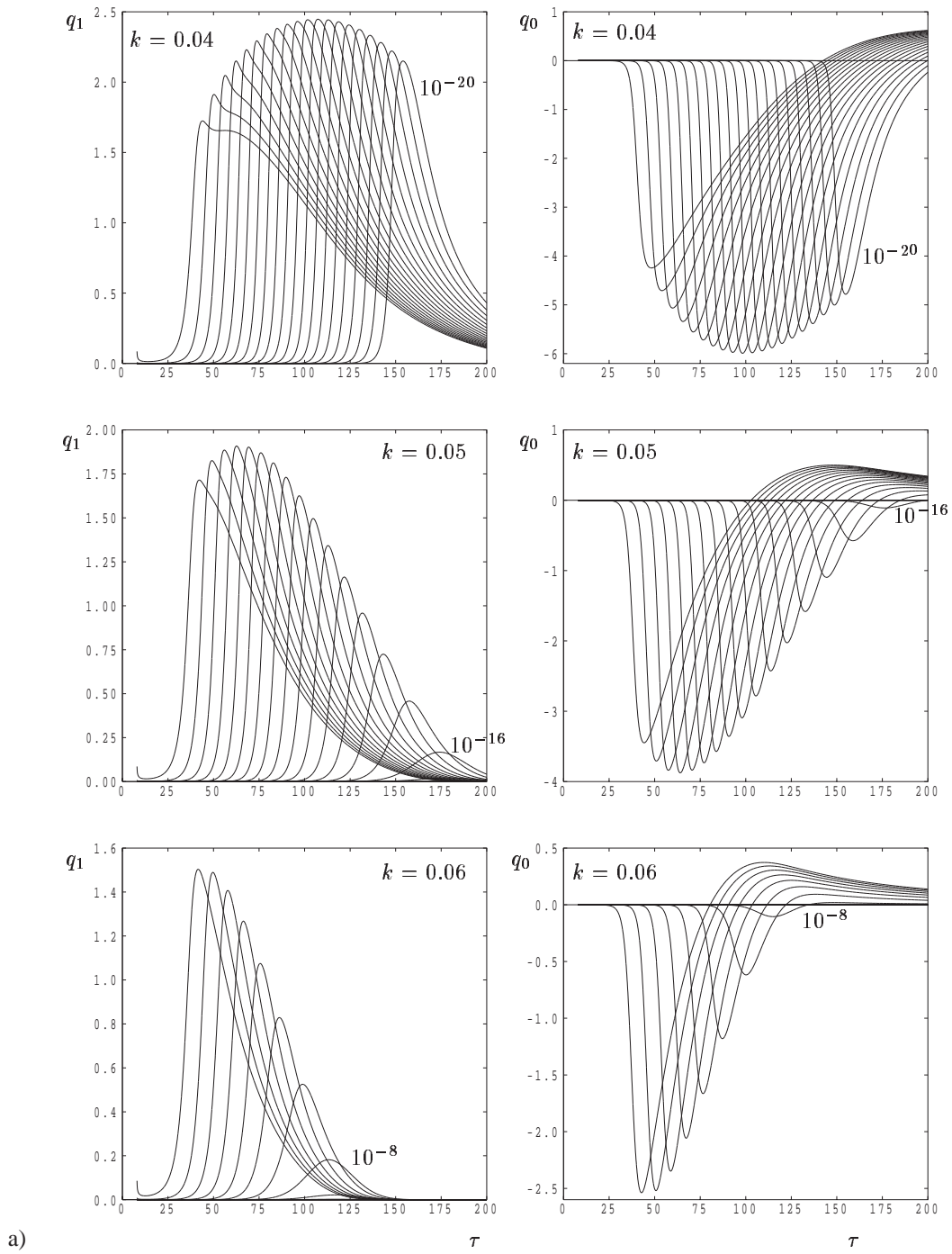
Figure 6. Variation with τ of q_1 (left-hand subfigures) and q_0 (right-hand subfigures) for various wave numbers between $k = 0.04$ and $k = 0.09$ and for the amplitudes $A = 10^{-1}, 10^{-2}, ..., 10^{-20}$. The value $\tau_0 = 8$ was used. The curve on the extreme left corresponds to $A = 10^{-1}$ in each case
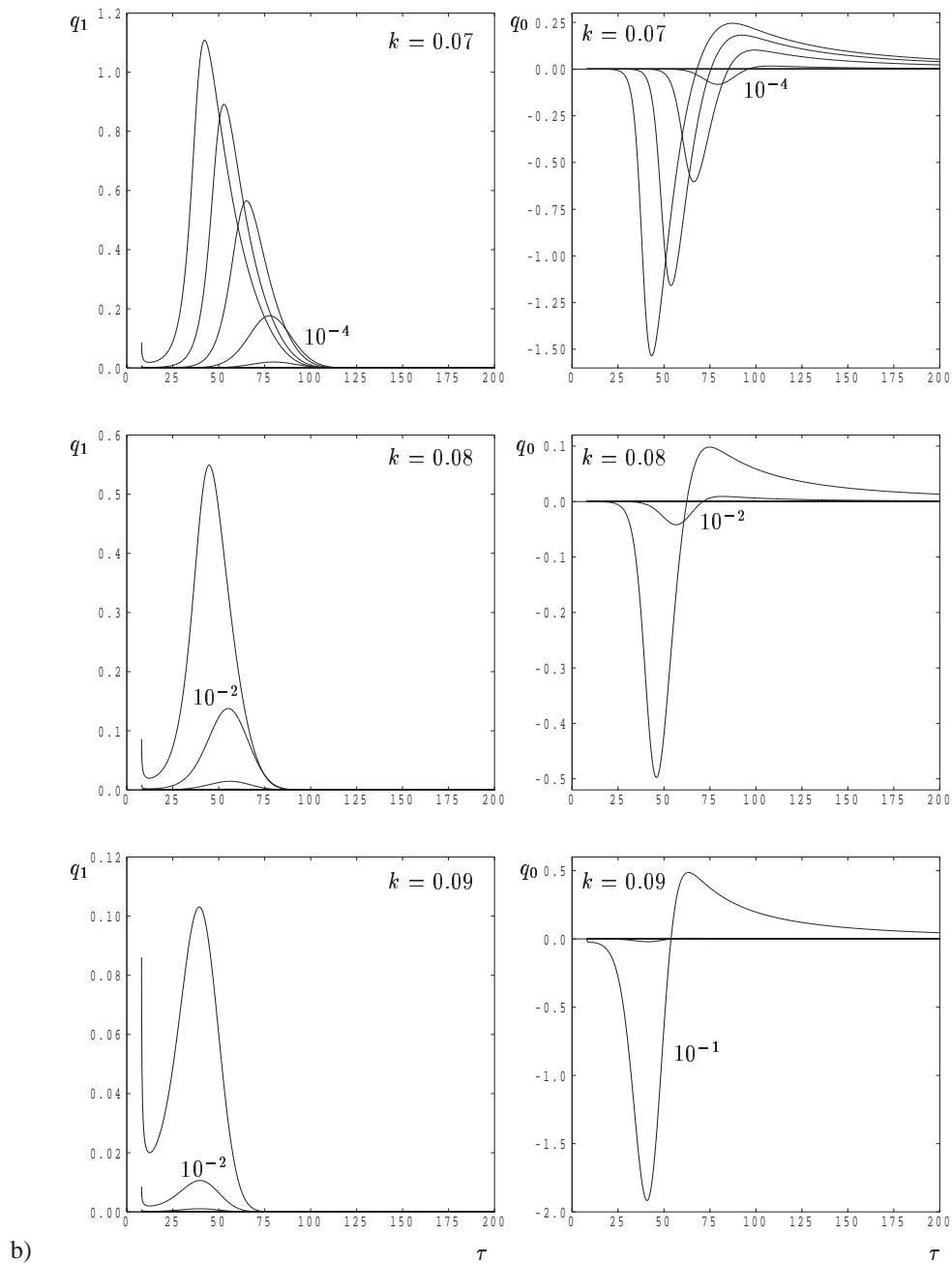
Figure 6. Cont'd

$k = 0.09$, the disturbance hardly enters the nonlinear regime, even when $A = 10^{-1}$.

A summary of the stability information contained in Fig. 6 is presented in Fig. 7. The abscissa of Fig. 7 is n, where the disturbance amplitude is $A = 10^{-n}$.

This figure shows the variation with n of what we shall call the nonlinear neutral points, denoted by τ_{nl}, and defined as being those values of τ where the variation of q_1 with τ takes either a maximum and minimum value, i.e., where $\frac{\partial q_1}{\partial \tau} = 0$. The lowest line
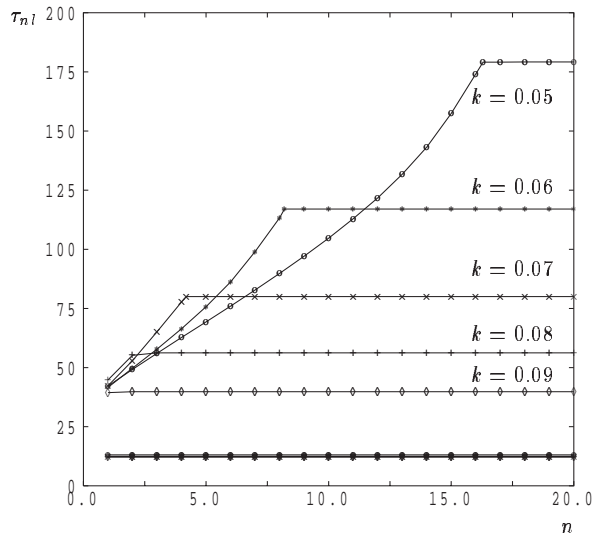
Figure 7. Variation in the values of the nonlinear neutral points, τ_{nl}, with $n = -\log_{10} A$ for different vortex wave numbers. The lines placed near to $\tau_{nl} = 13$ correspond to the onset of instability; the others correspond to the beginning of decay

in Fig. 7 appears to be a fairly thick line, but it is composed of all those lines corresponding to the onset of growth for each of the wave numbers considered. They form a fairly densely packed group because the onset times, as shown in Fig. 1, vary only slightly with k for these wave numbers. The remaining lines correspond to the times when restabilization occurs, i.e., to where the disturbance begins to decay again, as measured by q_1. Near to $n = 20$, which corresponds to $A = 10^{-20}$, the values of τ_{nl} do not vary with n because the disturbance always stays within the linear regime, and such horizontal lines correspond to the restabilization time for linear theory. However, the sloping lines show the times where nonlinear saturation causes premature restabilization. The case $k = 0.05$ is particularly severe, for disturbances as small as $A = 10^{-16}$ become highly nonlinear before the restabilization time for linear theory. The value of n at which the nonlinear restabilisation criterion gives way to the linear criterion and, in particular, its variation with k, can be seen easily in Fig. 7.

Effect of varying the initiation time

The nature of the evolving disturbance also depends on when the disturbance is introduced. Part I showed how the onset time depends on the initiation time while in the linear regime, but this conclusion is also true for nonlinear convection. Figure 8 shows the detailed evolution of q_1 with τ of an $A = 10^{-1}$ disturbance; the detailed values of q_1 show that the onset time increases with τ_0. A close-up view of the $k = 0.06$ case is shown in Fig. 9, where the onset times for smaller values of τ_0 are marked using filled circles, and where they may be seen clearly to increase with with increasing τ_0. Returning to Fig. 8, the essential linearity of the $k = 0.09$ case is quite evident even though $A = 10^{-1}$ is rather large. When τ_0 is small, the disturbance decays at first, and the onset time is a function of τ_0 since the shape of the disturbance changes with time; see the discussion in Part I. However, the time available for growth is limited and the restabilization time is clearly almost independent of τ_0. For the smaller wave numbers, however, both the onset and restabilization times are strong functions of τ_0, and there is a favoured value of τ_0 that maximizes the response in terms of q_1.

A summary of the stability properties of the solutions displayed in Fig. 8 is presented in Fig. 10. The wave numbers chosen correspond exactly to those in Fig. 8. In each subframe, the lower horizontal lines correspond to the onset criterion for linear theory, whereas the upper horizontal lines correspond to the restabilization time from linear theory. The diagonal line represents the initiation time τ_0, while the symbols indicate the calculated onset and restabilisation time for each τ_0 value.

When $k = 0.09$, we have the typical behaviour for linear theory that the onset time is roughly the larger of the onset time due to linear theory and τ_0, while restabilization takes place close to that time predicted by linear theory. The only exception is when the initiation time is later than the restabilization time, in which case the disturbance always decays. The curves for $k = 0.08$ show a slightly premature restabilization
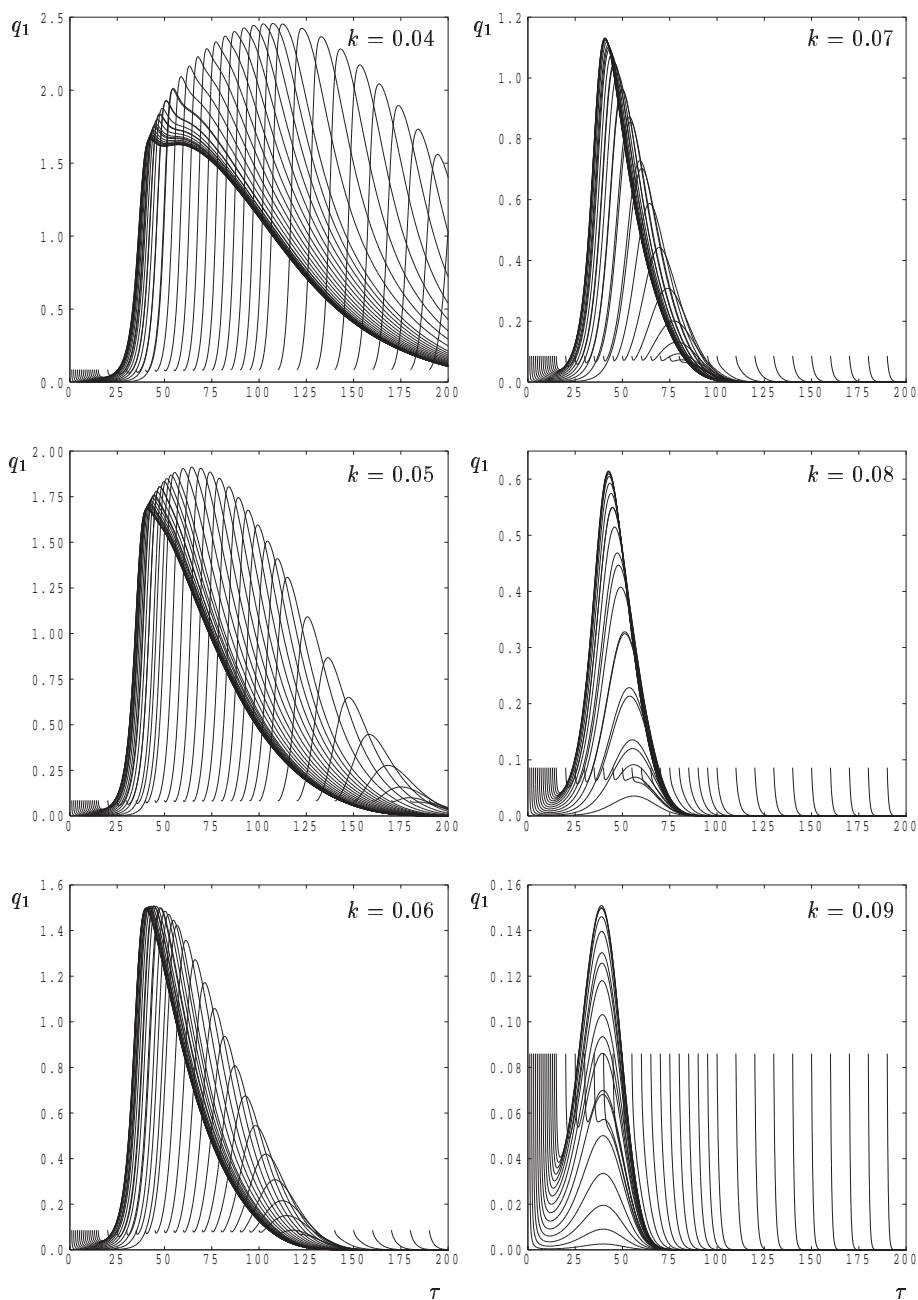
Figure 8. Variation of q_1 with τ for various values of τ_0 for different wave numbers between $k = 0.04$ and $k = 0.09$. In each case $A = 10^{-1}$ is the initial amplitude

when $2 \leq \tau_0 \leq 35$. It is clear that some nonlinear effects are present. For smaller wave numbers, restabilization can happen very early compared with linear theory, and, for large ranges of τ_0, it appears that growth occurs over a roughly constant range of values

of τ. When $k = 0.04$, the onset/restabilization criteria become a little more complicated. For example, when $\tau_0 = 20$, q_1 has two regions over which the disturbance grows. Preliminary extensions of the current work to smaller values of k suggest that the evolu-
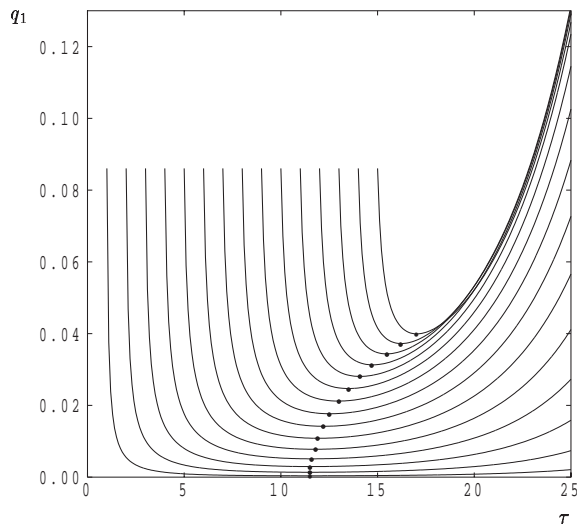
Figure 9. Close-up view of the $k = 0.06$ subfigure of Fig. 8. The solid circles denote where the slope of q_1 against τ is zero and mark the onset of instability

tion of disturbances becomes much more complicated in these cases. There opens up the possibility that mode 2, which is initiated as mode 1 grows and interacts with itself, may grow faster than mode 1 itself when k is small, and then establish itself as the stable mode — it is possible that the novel feature shown for $k = 0.04$ is associated with this scenario and it is intended to report on this aspect in due course.

Finally, we focus on one wave number, $k = 0.06$, and vary both the amplitude and initiation time. The results of extensive computations are shown in Fig. 11. The variation of τ_{nl} with τ_0 is depicted for the amplitudes $A = 10^{-1}$, 10^{-3}, 10^{-5}, 10^{-7}, and 10^{-9}. Here, the onset time is independent of A and the lowest symbols for each value of τ_0 corresponds to onset. Strongly nonlinear effects associated with $A = 10^{-1}$ reduce in effect as A decreases and restabilization happens later. When A is as small as 10^{-9}, we have returned to the linear regime once more.

CONCLUSIONS

We have investigated the nonlinear aspects of the evolution of two-dimensional cellular instabilities in a de-

veloping thermal boundary layer in a porous medium. This is an extension to the linearised stability analysis presented in Part I. In general we have found that the presence of nonlinearities serves to change the following features of the evolving disturbance: (i) nonlinear saturation causes the disturbance to begin to decay much earlier than is predicted by linear theory; (ii) a very strong change to the mean temperature profile is developed; (iii) alternate cells are either compressed toward the surface by inflow or are pushed away from the surface by outflow. It was also found that the time at which nonlinear saturation occurs depends quite strongly on the initial amplitude and the initiation time of the disturbance.

Although we have found premature decay of the evolving disturbance when it is in the nonlinear regime, the Darcy-Rayleigh number based on the growing thickness (in terms of y) of the basic temperature profile continues to grow, and therefore, the boundary layer continues to become increasingly unstable. It is therefore natural to ask how these two facts might be reconciled. An analogous set of studies by Rees (2001,2002,2003) on steady free convective boundary layer instabilities sheds some light on this. The first paper of these three considers linearized theory for the onset of streamwise vortex convection in a near-vertical free convective boundary layer. The second considers the nonlinear evolution of these vortices, while the third considers how these vortices are themselves destabilized. The general argument invoked is based on the fact that the evolving boundary layer appears to favour convection cells of aspect ratio roughly equal to 1. As the wave number and, hence, the wavelength of the cells must remain constant, the aspect ratio of the evolving cells continues to increase with distance from the leading edge until they are substantially different from unity. At this point, a further disturbance with a substantially lower wave number, but which is such that its aspect ratio is close to unity at this later time, will then begin to grow and take over as the new primary mode. Such a situation may be termed a subharmonic instability, as the new wave-
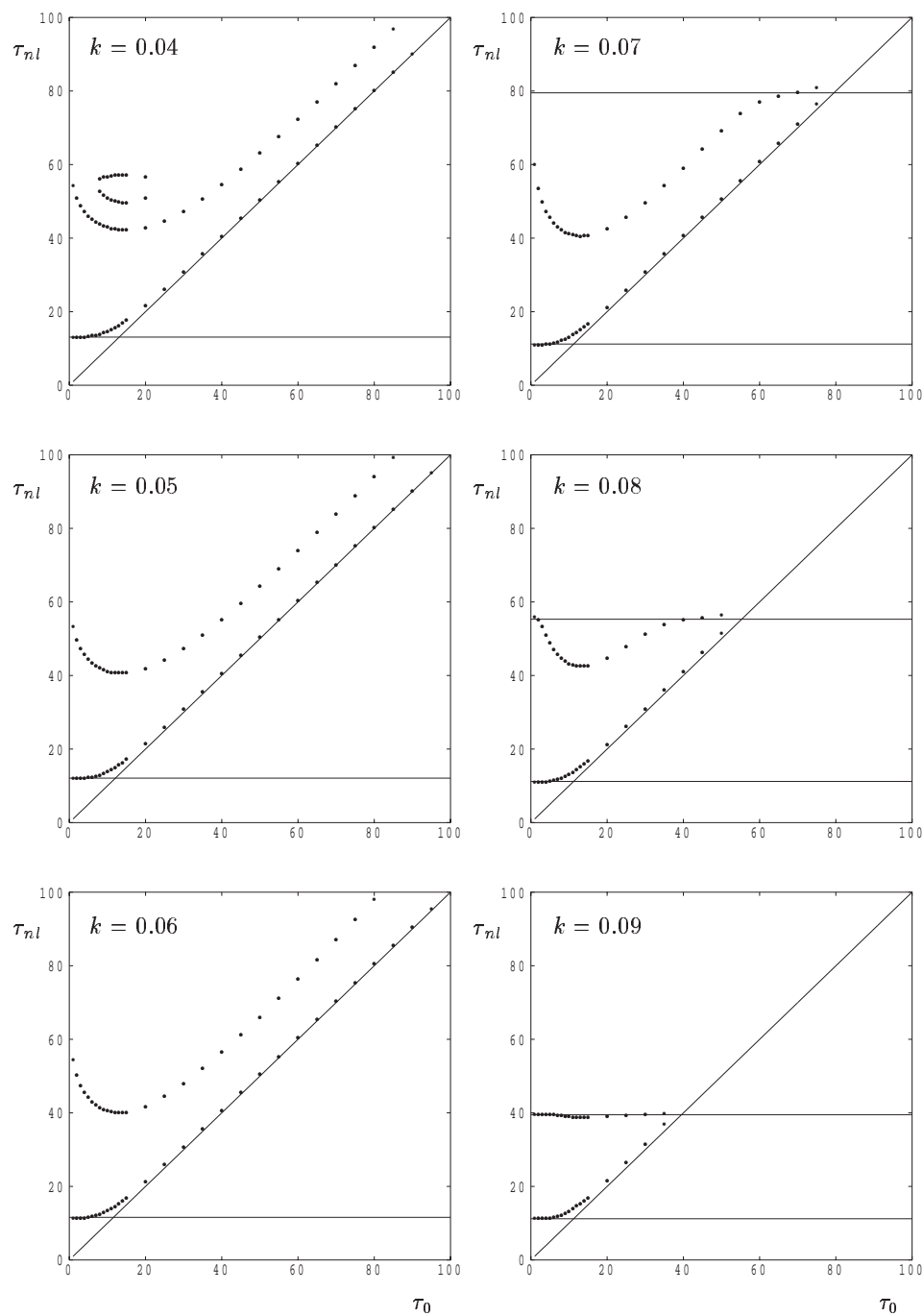
Figure 10. Variation of τ_{nl} with τ_0 for various values of the wave number, k. The amplitude of the initial disturbance is $A = 10^{-1}$. The horizontal lines depict the linear stability criteria given in Fig. 1, while the diagonal line shows where $\tau_{nl} = \tau_0$
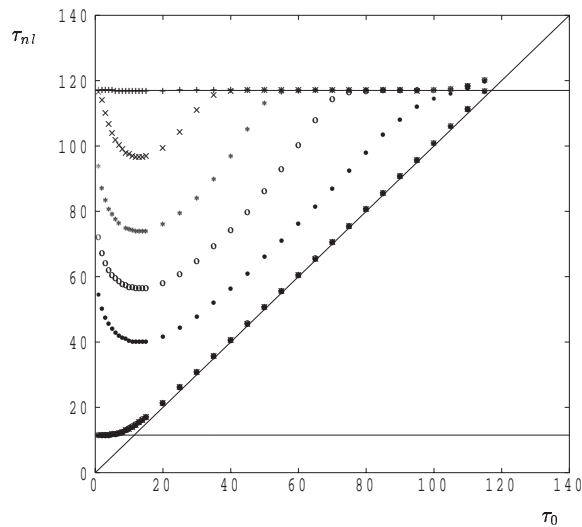
Figure 11. Effect of different disturbance amplitudes A on the nonlinear stability criterion for $k = 0.06$. The symbols, $\bullet$, $\circ$, $*$, $\times$, and $+$ refer to $A = 10^{-1}$, 10^{-3}, 10^{-5}, 10^{-7}, and 10^{-9}, respectively

length is likely to be double or triple the wavelength of the original disturbance. We intend to report on this aspect in future work.

ACKNOWLEDGMENT

REFERENCES

Kaviany, M., Thermal convective instabilities in a porous medium, *ASME J.Heat Tranfer*, vol. **106**, pp. 137–142, 1984.

Keller, H. B., and Cebeci, T., Accurate numerical methods for boundary layer flows 1. Two dimensional flows, *Proc. Int. Conf. Numerical Methods in Fluid Dynamics, Lecture Notes in Physics,* Springer, New York, 1971.

Kim, M. C., and Kim, S., Onset of convective instability in a fluid-saturated porous layer subjected to time-dependent heating, *Int. J. Heat Mass Transfer*, vol. **32**, pp. 416–424, 2005.

Kim, M. C., Kim, S., and Choi, C. K., Convective instability in fluid-saturated porous layer under uniform volumetric heat sources, *Int. Commun. Heat Mass Transfer*, vol. **29**(7), pp. 919–928, 2002.

Kim, M. C., Kim, S., Chung, B. J., and Choi, C. K., Convective instability in a horizontal porous layer saturated with oil and a layer of gas underlying it, *Int. Commun. Heat Mass Transfer*, vol. **30**(2), pp. 225–234, 2003.

Lewis, S., Rees, D. A. S., and Bassom, A. P., High wave number convection in tall porous containers heated from below, *J. Mech. Appl. Math.*, vol. **50**, pp. 545–563, 1997.

Rees, D. A. S., Vortex instability from a near-vertical heated surface in a porous medium. I Linear theory, *Proc. R. Soc. A.*, vol. **457**, pp. 1721–1734, 2001.

Rees, D. A. S., Vortex instability from a near-vertical heated surface in a porous medium. II Nonlinear theory, *Proc. R. Soc. A.*, vol. **458**, pp. 1575–1592, 2002.

Rees, D. A. S., Nonlinear vortex development in free convective boundary layers in porous media, *NATO ASI Proceedings*, Neptun, Romania, June 9–20, pp. 449–458, 2003.

Selim, A., and Rees, D. A. S., The stability of a developing thermal front in a porous medium. I linear theory, *J. Porous Media*, vol. **10**, no. **1**, pp. 2–10 , 2007.